John von Neumann Institute for Computing

Dissipative Particle Dynamics Simulations of Planar Amphiphilic Bilayers

Julian C. Shillcock, Reinhard Lipowsky

published in

NIC Symposium 2001, Proceedings,
Horst Rollnik, Dietrich Wolf (Editor),
John von Neumann Institute for Computing, Jülich,
NIC Series, Vol. **9**, ISBN 3-00-009055-X, pp. 407-417, 2002.

http://www.fz-juelich.de/nic-series/volume9

Dissipative Particle Dynamics Simulations of Planar Amphiphilic Bilayers

Julian C. Shillcock and Reinhard Lipowsky

Max-Planck-Institut für Kolloid-und Grenzflächenforschung
14424 Potsdam, Germany
E-mail: {shillcock, lipowsky }@mpikg-golm.mpg.de

The equilibrium structure and lateral stress profile of bilayer membrane patches are investigated using the Dissipative Particle Dynamics simulation technique. Although there are no attractive forces between the model amphiphiles, they spontaneously aggregate into planar bilayers under suitable conditions of concentration and amphiphile architecture. Pure bilayers of single-chain amphiphiles are simulated, and the amphiphile architecture and interaction parameters varied. We find that a strong chain stiffness potential is essential to create the degree of lamellar order typical in natural lipid membranes. The lamellar order of the bilayers is destabilised by reductions in the tail stiffness. The lateral stress profile across the bilayers contains detailed structure reflecting contributions from all the interaction potentials, as well as the amphiphile architecture. The stress profile is similar to that found in coarse-grained Molecular Dynamics simulations, but is here established at a fraction of the computational cost. Dissipative Particle Dyamics therefore allows the study of equilibrium behaviour of amphiphilic membranes hundreds of times larger than can be achieved using Molecular Dynamics simulations, and opens the way to the study of complex mesoscopic cellular phenomena.

1 Introduction

Lipid bilayer membranes surround living cells, protecting their interior from the outside world. They are much more than a static structural component, however, in that their composition and dynamics influence membrane-bound proteins, and contribute to the remarkable material properties of cells such as red blood cells[1]. Bilayer membranes also surround artificial vesicles, and have been constructed out of non-biological amphiphiles[2,3], and diblock copolymers[4]. These membranes continually undulate owing to the thermal motion of their constituent lipids. Thermal forces combine with specific molecular forces to create complex, dynamic, multi-component systems[5]. Dynamic processes taking place within a membrane can involve co-operative changes over distances large compared to the molecular size, and occur on time-scales much longer than molecular vibrational periods.

The complexity of natural membranes has led experimentalists to focus on simpler model systems:lipid bilayer vesicles[5,6]. These are often composed of a single type of amphiphile, and usually lack embedded inclusions. Much progress has been made in the last decade in experiments designed to probe the vesicle membrane's material properties. The area stretch modulus of pure stearoyloleoylphosphatidylcholine (SOPC) vesicles and SOPC/cholesterol mixtures has been measured using micropipette aspiration[7], and is found to increase on adding cholesterol as a cosurfactant. The lateral diffusion of lipids in a vesicle membrane[8] and the membrane viscosity[9] have both been recently determined. Detailed studies[10] have been published of the dependence of the bilayer elastic bending and area stretch moduli on lipid tail length and the degree of unsaturation. Amphiphilic diblock copolymers have been shown to form vesicles that are an order of magnitude stronger, and

less permeable to water, than natural phospholipid bilayers[4]. Such toughened vesicles, or polymersomes, offer greater control over the membrane material properties than lipid vesicles owing to the possibility of cross-linking the copolymers and changing the block size or molecular weight.

We have used the Dissipative Particle Dynamics (DPD) simulation method to investigate the structure and lateral stress profile of bilayer membranes containing approximately 3200 amphiphiles as a function of the amphiphile architecture and interaction parameters. This represents a membrane patch at least one order of magnitude larger than previously published results[12–15], and allows us to study the membrane's mesoscopic properties while the (presumably) irrelevant short length-scale motions of the individual amphiphiles are averaged out. The DPD technique was first introduced almost a decade ago[16], and recent articles provide a comprehensive survey of the method[17,18].

The paper is organised as follows. We first provide the motivation for our work and then briefly review the Dissipative Particle Dynamics simulation technique, referring the interested reader to Ref. 17 for a detailed description. Then we present results on the equilibrium bilayer structure and stress profile of amphiphilic bilayers as a function of the amphiphile architecture and interaction parameters. Finally, we discuss the implications of this work for simulating complex processes in lipid bilayers.

2 Motivation

Experiments on complex biomembranes have created a demand for a theoretical understanding of the dependence of membrane material properties on the constituent amphiphile's molecular structure and membrane composition. Because mean-field and lattice-based models[11] ignore membrane undulations, restrict amphiphile headgroups to a planar interface, and cannot easily incorporate the effects of arbitrary molecular architecture, attention has turned to predicting material properties using coarse-grained Molecular Dynamics (MD) simulations. This approach has been used to extract the area compression modulus and bending modulus of single-component lipid bilayers, and their lateral stress distribution[12]. The latter quantity is believed to be important in modulating membrane-bound protein behaviour[19]. Recently, coarse-grained MD simulations have been used to compare the equilibrium structure of a dimyristoylphosphatidycholine bilayer[15] to that obtained from atomistic simulations. This provides the opportunity to move up in length-scale towards the mesoscopic regime. However, a major drawback of these MD simulations is that they are restricted by current computing technology to membrane patches containing only a few hundred amphiphiles plus the requisite solvent molecules. Mesoscopic simulation techniques, such as DPD, offer the possibility of extracting information about the material properties of biomembranes, and other complex fluid systems, well beyond the length and time scales achievable by MD simulations. Our aim in this work is to determine whether DPD simulations can take the investigation of membrane material properties to length and time scales beyond those achievable in coarse-grained MD simulations, whilst still exhibiting the structure found in lateral stress profiles. Given that a micron-size vesicle can contain from one million to a billion amphiphiles, and that a few percent of its surface area is involved in processes such as pore formation or fusion events, the ability to model large systems is essential if these processes are to be studied using computer simulations.

3 Dissipative Particle Dynamics Simulation Method

The elementary units in a DPD simulation are fluid elements or *soft beads*. A bead represents a volume of fluid that is large on a molecular scale, and hence contains at least several molecules of the fluid, but still macroscopically small. Beads interact via effective forces chosen so as to reproduce the hydrodynamic behaviour of the fluid without reference to its molecular structure. DPD differs in this respect from MD simulations, in which the forces are chosen to model the inter-molecular interactions of a system as accurately as possible. Forces in DPD are pairwise additive, conserve momentum, have no hard core and are short-ranged, the range of the force defining the size of the soft beads. All beads have the same mass, m_0, and radius, r_0, unless otherwise stated, and these set the mass and length scales in the simulation. A time-scale must be extracted from the dynamics of relevant processes in the simulated fluid, such as the diffusion of a micelle's centre of mass, or the in-plane viscosity of a bilayer membrane. Because we study equilibrium properties of the bilayers, we estimate the time-scale of the simulations from the generic time, $t_0 = \sqrt{m_0 r_0^2 / k_B T}$, set by the bead mass and radius and the system temperature, where k_B is Boltzmann's constant and the temperature T is defined in Ref. 17. We take the diameter of one DPD bead as 1 nm and assume that it has the density of water at room temperature, $T = 300K$. The simulation time-step then corresponds to 5 ps, and a typical run of 10^5 steps is equivalent to approximately a microsecond of real time.

Simulations take place within a cuboidal box of constant volume $V = L_X.L_Y.L_Z$, where L_X, L_Y, L_Z are the simulation box side lengths in units of the bead diameter, r_0. Periodic boundary conditions are used in all three dimensions to minimise edge effects. The simulation box is filled with beads to the chosen density which represents ρ beads/unit volume. We are interested in studying the properties of a single bilayer in water. The number of amphiphiles in the bilayer, N, is determined by the box area, $L_X.L_Y$, and the desired projected area per amphiphile, A_{pr}/N according to $N = \frac{2.L_X.L_Y}{A_{pr}/N}$. Because the bead radius, r_0, defines the length scale for the simulations, we quote dimensional quantities in their dimensionless form, e.g., the area per amphiphile is A/Nr_0^2. In a similar manner, the mass and time scales are obtained from the bead mass and radius, and the system temperature.

Various polymer architectures are used to represent bilayer-forming amphiphiles. They are composed of hydrophilic head beads, designated H, and hydrophobic tail beads, designated C. The simplest architecture has a single H bead attached to a linear chain of C beads. The number of tail beads is varied to investigate the dependence of bilayer properties on the degree of amphiphile hydrophobicity. An amphiphile containing one head and n tail beads is represented, using an obvious symbolism, as HC_n. The amphiphiles are contained within bulk solvent composed of W beads. Each solvent bead represents a small volume of bulk water consisting of several molecules. Because each W bead represents several molecules of solvent, there is no explicit modelling of hydrogen bonds or entropic forces. The interactions between beads in DPD simulations are to be interpreted as a coarse-graining of a fluid rather than a simulation of the molecules of a fluid. In this way, only structure and behaviour that occurs on a length-scale larger than the elementary beads in the simulation have physical relevance.

We refer to the polymers as surfactants or amphiphiles rather than lipids both to emphasise the generality of the simulation technique, and to avoid suggesting that the model

amphiphiles should be viewed as atomically-detailed representations of the complex structure of lipid molecules. In the same vein, we refer to DPD beads connected by springs as polymers rather than molecules, but this is not meant to imply that the polymers are necessarily long nor that they are composed of identical repeating units. The interpretation of a polymer composed of DPD beads requires some care. We take the view that the head bead in a model lipid represents the hydrophilic glycerol-phosphate-head region while each tail bead represents several methyl groups in a hydrocarbon chain. In this view, each hydrophobic bead represents, say, 2 to 5 methyl groups. The same interpretation applies to non-biological amphiphiles, such as alkyl phosphate surfactants[2] that consist of an single carbon chain attached to a phosphate head group.

4 Results on Equilibrium Structure of Bilayer Membranes

The simplest amphiphile architecture that is found to self-assemble into a bilayer consists of a single, hydrophilic head bead attached to a linear chain of hydrophobic tail beads designated HC_n. A snapshot of a bilayer composed of HC_6 amphiphiles is shown in Figure 1. The simulation box size is $V/r_0^3 = 32^3$, and the overall bead density is $\rho r_0^3 = 3$ giving approximately 100,000 beads of all types. A bilayer readily self-assembles when the amphiphiles are initially randomly distributed in water for surfactant number fractions in the fairly restricted range of $3 - 6\%$. Below this range micelles occur, and above it complicated three-dimensional structures are formed (data not shown). The amphiphiles aggregate into a bilayer because of the strong repulsion between their tail beads and the solvent beads, mimicing the hydrophobic force of, for example, lipid molecules in water. Because of the large parameter space of the simulations, we investigate the effects of just a few parameter combinations. Given three bead types (H, C and W) there are 6 independent bead-bead interaction parameters. Their values are: $a_{HH} = a_{CC} = a_{WW} = 25$, $a_{HW} = 35$, $a_{HC} = 50$, $a_{CW} = 75$. The self-interactions are determined by the requirement that a pure fluid of each bead type has the compressibility of water[17], while the unlike bead-bead interactions are varied to represent the degree of solubility of one species in another, or the hydrophobicity of the hydrocarbon chain of the amphiphiles. The beads are connected into semi-flexible polymers using a bond potential and a chain bending potential that contribute two more parameters each. We reduce these by fixing the spring constant and unstretched bond length to $k_2 r_0^2/k_B T = 128$ and $l_0 = 0.5 r_0$ respectively, and the preferred bond angle to 0. This choice of values is explained later. This leaves 4 parameters to be investigated: a_{HC}, a_{HW}, a_{CW} and $k_3/k_B T$ in addition to the number density of amphiphiles which is set by the projected membrane area, $A_{pr}/N r_0^2$ and the simulation box size. We have not investigated the effects of varying the dissipation coefficients because they should be irrelevant for the equilibrium structures we are interested in. Instead, they are chosen according to the procedure in Ref. 17 to yield a well-ordered bilayer. Because of the isotropy of the simulation box, bilayers do not always assemble with the same orientation, but to simplify the discussion we refer to the bilayer normal as the Z axis in all our results. A small bilayer containing 830 amphiphiles in an area 16^2 readily self-assembles from an initially random configuration in 20000 time-steps (data not shown). Because self-assembly of bilayers has been studied previously[12–15] and we are interested in measuring equilibrium properties of large membranes, we pre-assemble the amphiphiles into a planar bilayer, and allow it to relax to an equilibrium state before constructing ensemble averages of observables.

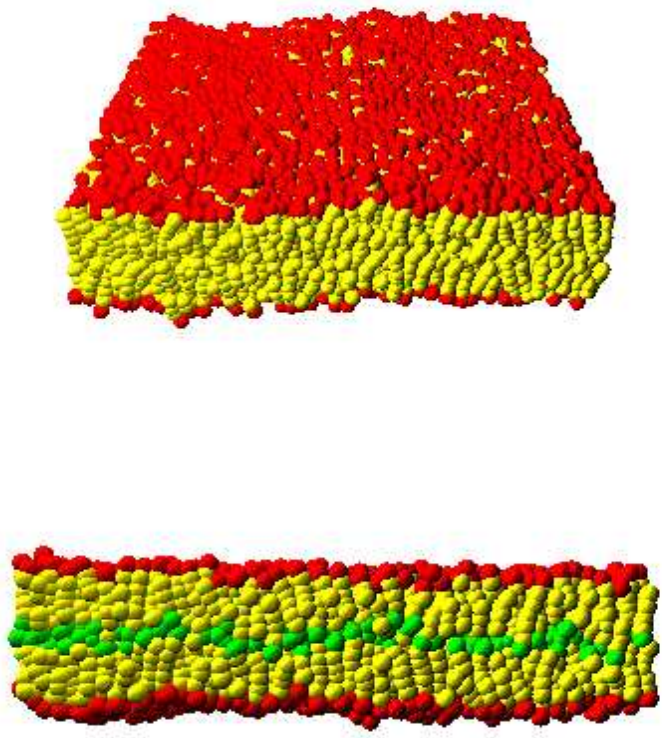

Figure 1. Snapshots of a bilayer containing 3321 HT_6 amphiphiles. The simulation box has size $(32r_0)^3$, and the bead density is $\rho r_0^3 = 3$ giving almost 100,000 beads of all types. The area-per-amphiphile is $A_{pr}/Nr_0^2 = 0.62 \pm 0.05$ leading to a surface tension of $\sigma = -0.03 \pm 0.1$. The amphiphile head beads are dark grey, and the tail beads are light grey. The average membrane width, measured from the centre of the head beads of one monolayer to those of the other, is $< \ell_{me}/r_0 >= 6.61 \pm 0.01$. Water beads are invisible for clarity. In the lower snapshot the terminal tail bead is coloured darker to demonstrate that the amphiphiles terminate near the bilayer midplane. The L_α order of the bilayer is evident, and the two monolayers are not very inter-digitated. Thermally-excited undulations are small here because of the chain bending stiffness of the amphiphiles.

The bilayer shown in Figure 1 contains 3321 HC_6 amphiphiles and has a relaxed area per amphiphile of $< A/Nr_0^2 >= 0.63 \pm 0.01$, and an approximately zero surface tension, $\sigma r_0^2/k_BT = -0.03 \pm 0.1$ (see next section for the measurement of surface tension). The snapshots in Fig. 1a and 1b come from separate simulations with identical parameters, but the terminal tail bead is coloured differently from the intermediate tail beads in 1b to show that the amphiphiles are approximately straight and terminate near the bilayer midplane. We measure the bilayer width and area from a triangulation of the two monolayer surfaces. A rectangular grid is placed over the simulation XY plane and the amphiphiles are assigned to grid cells according to the X,Y coordinates of their head beads. The upper monolayer contains those amphiphiles whose head Z coordinates are greater than their tail Z coordi-

nates. The lower monolayer contains all other amphiphiles. This defines the number of amphiphiles in each monolayer. The average Z coordinate of the head beads in each grid cell for each monolayer is used to define the height of the monolayers at each point (X,Y). This procedure yields a two-dimensional height field, $h(X, Y)$, for each monolayer. The bilayer width, ℓ_{me}, is the difference between these heights averaged over all grid points, and the surface area of each monolayer, A, is the sum of the areas of the triangles composing it. The grid cell width is typically twice the bead radius, so that there are at least several amphiphiles per cell. This smears out the excursions of single amphiphiles from the monolayers ensuring that the monolayer area is not overly sensitive to small-scale fluctuations.

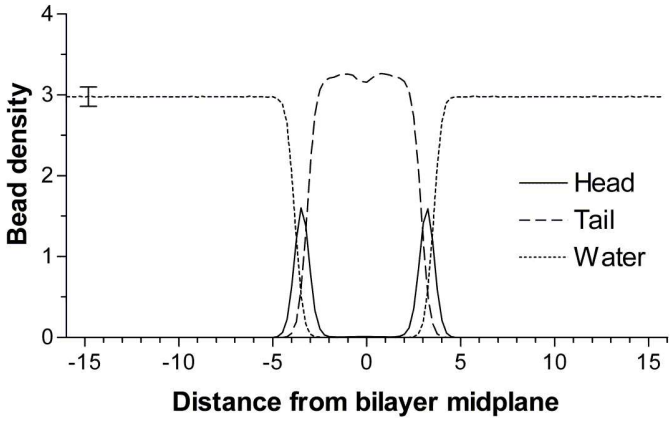

Figure 2. Bead density profiles for head and tail beads in the bilayer of Fig. 1 and the bulk water. The simulation box is divided into 128 slices of thickness $r_0/4$ parallel to the bilayer surface, and the time average of the number of beads of each type in the slices is used to generate the density profiles. Water is excluded from the bilayer interior by the strong hydrophobic repulsion of the tail beads, and the head beads are localised at the water-hydrophobic interface. The tail bead profileincludes all the tail beads, and shows that the density in the hydrophobic region is uniform except for a small dip at the bilayer midplane. All error bars are similar to the one shown and indicate the statistical accuracy of the ensemble averages extracted from the simulations.

The lateral density profiles of the hydrophobic and hydrophilic beads in the HC_6 bilayer, together with the water beads, are shown in Figure 2. It is clear from Figures 1 and 2 that the amphiphiles terminate close to the bilayer midplane, with the final tail bead confined to that region, and that they exhibit strong L_α order. The profiles are calculated by averaging the bead densities over thin slices (of width $r_0/4$) parallel to the bilayer surface. The water is excluded from the hydrophobic region of the bilayer by the strong tail-water repulsion, whereas the head beads can sometimes penetrate to the centre, although this is hardly visible in this figure. Two effects contribute to this penetration: amphiphiles can burrow their way through the bilayer emerging into the apposed monolayer, a process known as "flip-flop"; and the thermally-excited undulations of the bilayer lead to density profiles that include contributions from non-planar bilayer configurations. The tail bead

density shows a small dip at the midplane of the bilayer, indicating that the monolayers are not significantly inter-digitated. Bilayers composed of linear amphiphiles HC_n with $n = 4 - 10$ exhibit these general properties, although the shape fluctuations are stronger for shorter-chain amphiphiles. Amphiphiles containing four or more tail beads are not observed to leave the bilayer and exchange with the solvent on the time-scale of the simulations, which is of the order of microseconds.

Although a bilayer forms from HC_n surfactants for a wide range of tail-water repulsions, a_{TW}, two constraints should be satisfied before the simulated bilayer has properties that match the typical structure of a lipid bilayer. The average amphiphile end-to-end length should be approximately one half of the bilayer width, so that the two monolayers do not interdigitate; and the amphiphiles should be straight and oriented along the bilayer normal. We present results for a region of the simulation parameter space satisfying these constraints by adjusting the bond stretching and stiffness potential parameters. Under these constraints, the amphiphile length can be meaningfully compared to that of lipid molecules, and the bilayer width scales linearly with the amphiphile tail length. The end-to-end length, L_{ee}, of an HT_n amphiphile is measured from the centre-to-centre distance from the H bead to that of the last T bead. Two bond types are present in these amphiphiles: HT and TT although, for simplicity, both types have the same bond strength parameters of $k_2 r_0^2/k_B T = 128, l_0/r_0 = 0.5$. These values yield average bond lengths of $< l_{HT}/r_0 >= 0.62 \pm 0.01$ and $< l_{TT}/r_0 >= 0.55 \pm 0.01$. The larger $< l_{HT}/r_0 >$ length reflects the repulsion of the head from the tail beads, and its greater freedom to fluctuate into the adjacent water than is possessed by the tail beads deeper in the hydrophobic bulk. The standard deviation of the bond lengths is less than 2% for all tail lengths and bilayer tensions. The amphiphile end-to-end length for the tensionless HT_6 bilayer is $< L_{ee}/r_0 >= 3.23 \pm 0.01$, which can be compared with the bilayer thickness $< \ell_{me}/r_0 >= 6.61 \pm 0.01$, showing that the two monolayers are not inter-digitated.

The end-to-end length grows linearly with the number of tail beads for all HT_n amphiphiles for a fixed bending stiffness $k_3/k_B T$ (data not shown) and is only slightly affected by the tension on the bilayer in the regime we study. It decreases slowly as the projected area per amphiphile, $A_{pr}/N r_0^2$, increases, with the decrease being larger for longer amphiphiles. For HT_8 amphiphiles, it decreases from $< L_{ee}/r_0 >= 4.28 \pm 0.01$ for $A_{pr}/N r_0^2 = 0.60$ to $< L_{ee}/r_0 >= 4.24 \pm 0.005$ for $A_{pr}/N r_0^2 = 0.64$. The absence of a corresponding variation in the bond lengths indicates that this shortening occurs by the bonds rotating relative to each other. Such rotations are resisted by the amphiphile chain stiffness potential discussed next. The surface tension increases from $\sigma r_0^2/k_B T = -3.0$ to $\sigma r_0^2/k_B T = 7.3$ over this span of areas indicating that HT_8 bilayers are quite rigid. All of our results for tensionless bilayers are taken from the regime $< \ell_{me}/L_{ee} >\approx 2.0$, in which the monolayers are not significantly interdigitated. Bilayers composed of HT_6 or longer amphiphiles are quite rigid and show only small shape fluctuations even close to zero surface tension.

At small values of $A_{pr}/N r_0^2$, the HT_4 membranes show substantial undulations, the fluctuations being gradually suppressed for amphiphiles with longer tails. In addition, a tensionless state could not be found for HT_4 bilayers simply by reducing the projected area because some amphiphiles inverted and buried their heads inside the hydrophobic region generating a positive surface tension. A well-ordered bilayer forms with a projected area of $A_{pr}/N r_0^2 = 0.70$, and surface tension $\sigma r_0^2/k_B T = 0.013 \pm 0.016$, when the

head-water repulsion parameter is decreased from $a_{HW} = 35$ to $a_{HW} = 27$, keeping all other potential parameters unchanged. Increasing A_{pr}/Nr_0^2 for all bilayers composed of HT_n amphiphiles reduces their shape fluctuations and width and, beyond a certain point, ruptures the membranes by the appearance of a pore. The amphiphiles around the pore rim reorient so as to shield their hydrophobic tails from the surrounding solvent (data not shown). Although interesting as a possible model of pore formation, we do not investigate bilayer rupture further here.

In the absence of chain stiffness, $k_3/k_BT = 0$, stable bilayers are formed in which the amphiphile tails represent (almost) freely-jointed chains, but the hydrophobic region lacks the characteristic L_α order of lamella phase lipid bilayers. The hydrophilic head beads also show a tendency to penetrate into the hydrophobic interior, although this effect decreases as the chain stiffness increases. A chain bending stiffness of $k_3/k_BT = 20$, and a preferred angle of $\phi_0 = 0$, causes the amphiphiles to align approximately parallel to the bilayer normal as seen in Figure 1. The linearity of the amphiphile chains may be estimated from the angle between adjacent bonds averaged over the chain length. More specifically, an orientational order parameter may be defined as the second Legendre polynomial of the scalar product of adjacent bond vectors. In the absence of a bending stiffness potential this order parameter is close to zero. With the above-mentioned values of $k_2r_0^2/k_BT = 128, l_0/r_0 = 0.5$ and $k_3/k_BT = 20, \phi_0 = 0$, the order parameter for amphiphiles containing from 4 to 10 tail beads is always in the range $0.8 - 0.9$.

5 Lateral Stress Profile for Bilayers of Linear Amphiphiles

Lipid bilayers around cells and vesicles are often close to a tension-free state. The distribution of stresses within the bilayer is not, however, uniform. Recent calculations[19] indicate that the presence of cosurfactants, and hydrocarbon chain stiffness due to unsaturated C-C bonds, modulate the membrane stress distribution. We have measured the stress distribution within the model bilayers as a function of amphiphile tail length and stiffness.

The calculation of the stress tensor for a system composed of point particles interacting via continuous potentials is described in Ref. 12, which extends earlier work of Schofield and Henderson[20]. In this method, the contributions to the stress profile of the bead-bead interactions, bond stretching and bond bending stiffness potentials are averaged over thin slices parallel to the bilayer surface. We define the stress profile, $\sigma(z)$, as the difference of the normal and lateral components of the stress tensor summed over all potentials. For further details of the calculation, the reader is referred to previous work[12]. The stress profile for the HT_6 bilayer described in Section A is shown in Fig. 3, and exhibits very similar structure to that seen in the MD simulations of Ref. 12. However, the absence of Lennard-Jones potentials in our simulations does not visibly modify the stress profile, indicating that the infinite barrier of Lennard-Jones potentials is not essential for capturing the stress profile structure in mesoscopic simulations. The integral of $\sigma(z)$ across the bilayer yields the surface tension. We approximate this integral by a summation across the whole simulation box in the Z direction because the contribution from regions containing only solvent vanishes. Figure 4 shows that the surface tension of bilayers composed of HT_5 to HT_{10} amphiphiles increases as A_{pr}/Nr_0^2 increases. The increase is steepest for the longer amphiphiles, and becomes sub-linear at large values of the projected area.

Reducing the tail bending stiffness for HT_6 amphiphiles to $k_3/k_BT = 10$, while

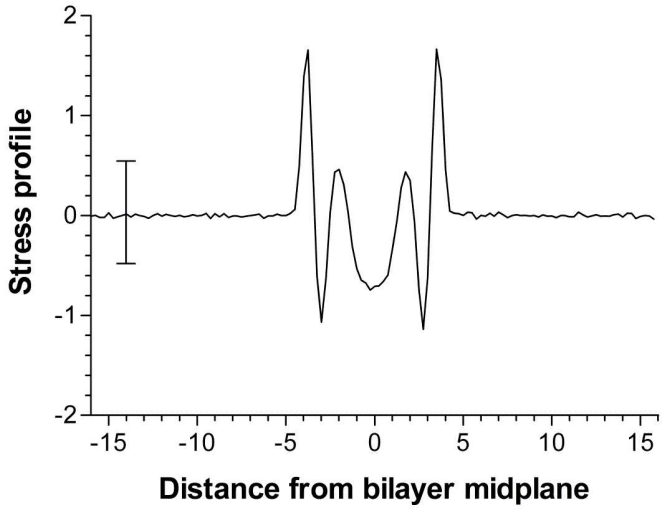

Figure 3. Stress profile for the HT_6 bilayer shown in Fig. 1. The total stress is the sum of three contributions: the repulsion potentials between head, tail and water beads; the Hookean spring potentials connecting adjacent beads in the amphiphiles, and the chain stiffness potential between adjacent triples of hydrophobic beads. The outer positive peaks at the monolayer-water interfaces are due to the repulsion between the hydrophobic tail beads and the hydrophilic head beads and water. The adjacent negative troughs arise from the Hookean bond potential compressing the amphiphiles, while the inner positive peaks near the monolayer midplanes are due to the chain stiffness potential.

keeping all other parameters constant, causes the bilayer shown in Fig. 1 to swell as some amphiphiles invert so that their heads are buried in the hydrophobic region. This reduces the lamella order of the tails to 0.7, and creates a large positive surface tension, $\sigma r_0^2/k_BT = 1.62$, across the bilayer. The surface tension remains positive as the projected area is varied, although it reaches a minimum, and the bilayer regains some of its ordered nature, for $A_{pr}/Nr_0^2 = 0.7$, at which point the mean bilayer width is $< \ell_{me}/r_0 >= 5.71 \pm 0.03$. The bilayer may be restored to a tensionless state by reducing the head-water repulsion parameter, a_{HW} to 30, and increasing the projected area to $A_{pr}/Nr_0^2 = 0.71$, but this leaves the chain order in the hydrophobic region at the reduced value of 0.7, and the bilayer width at $< \ell_{me}/r_0 >= 5.72 \pm 0.02$. This result shows that the chain bending stiffness and amphiphile head-water repulsion parameters cannot be independently varied in a simulation to produce a tensionless bilayer, but that they play effectively opposite roles in controlling the tendency of amphiphiles to invert and bury their heads in the hydrophobic region. Reducing the chain stiffness of amphiphiles in a tensionless bilayer requires a simulaneous reduction in their head-water repulsion and an increase in the projected area to restore the bilayer to a tensionless state. The surface tension for bilayers near their tensionless state is very sensitive to changes in the area per amphiphile: adding or removing just three amphiphiles from the tensionless HT_6 bilayer of Fig. 1, which contains 3321 amphiphiles, changes its surface tension from $\sigma r_0^2/k_BT = -0.03 \pm 0.1$ to $\sigma r_0^2/k_BT = -0.15$ and $\sigma r_0^2/k_BT = 0.10$ respectively. The

surface tensions for an HT_8 bilayer containing $3368, 3365, 3362$ amphiphiles in a fixed simulation box of size $(32/r_0)^3$ are $\sigma r_0^2/k_BT = -0.24, 0.024, 0.21$ respectively. Away from the tensionless state, the surface tension changes more rapidly with projected area for longer tail amphiphiles. Similarly, although the equilibrium bilayer structure is insensitive to the exact value of the tail-water repulsion parameter in the range $a_{TW} = 65 - 85$, the width of the bilayer changing by less than 0.2% to 6.60 ± 0.01 and 6.62 ± 0.01 for the two extreme values, the peak heights in the lateral stress profile, and therefore the surface tension, are very sensitive to this parameter. Changing a_{TW} for the bilayer of Fig. 1 to 65 and 85 changes the surface tension from approximately zero to $\sigma r_0^2/k_BT = -0.58, 0.55$ respectively, all other parameters being constant. This has the effect of moving the tensionless bilayer state to higher and lower projected areas respectively.

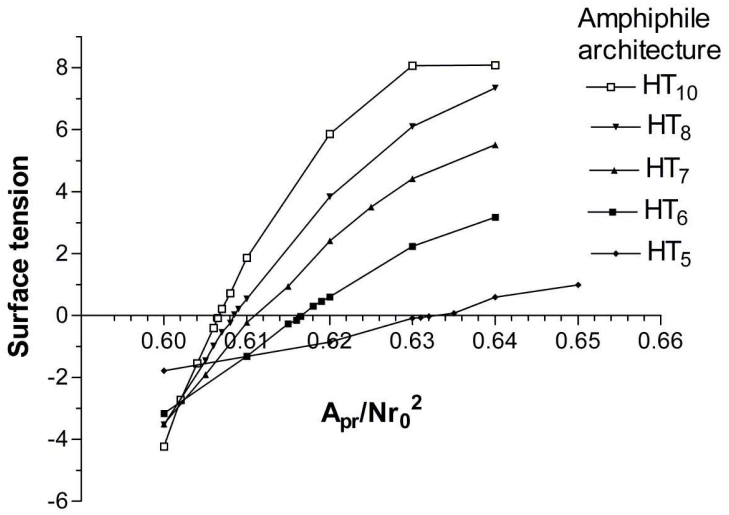

Figure 4. Variation of the surface tension with the projected area per amphiphile, A_{pr}/Nr_0^2, for bilayers composed of HT_n amphiphiles for several tail lengths. The surface tension is obtained by integrating the stress profile across the bilayer as described in the text. The lines connecting the points are only to guide the eye but show that the surface tension varies linearly around its zero point, and shows a sub-linear dependence on area at large projected areas. The preferred area per amphiphile, at which the surface tension vanishes, decreases as the amphiphile tail length increases.

6 Concluding Remarks

A major goal of computer simulations is to predict the material properties of mesoscopic, or possibly macroscopic, aggregates given only the elementary molecular constituents composing them. Although, perhaps, less useful for simulating interactions between hard colloidal particles in solution, DPD shows great promise when applied to soft complex fluids. We have shown that model amphiphiles consisting of a hydrophilic headgroup attached to

a hydrophobic tail form planar bilayers whose density profile and lateral stress distribution, and the dependence of these properties on the tail length, agree at least qualitatively with experiments and previous coarse-grained MD simulations. The task of capturing just those microscopic properties of amphiphiles that give rise to the material properties and dynamical behaviour of lipid bilayers or polymersomes is a challenge whose solution will have direct applications to chemistry, materials science and medicine. We believe that DPD is highly suited to complex fluid simulations because it allows the mesoscopic behaviour of large systems to be followed for long times at relatively small computational cost.

Acknowledgments

Membrane simulations were performed with the aid of a grant of computer time provided by the NIC of the Research Centre Jülich.

References

1. R. Lipowsky and E. Sackmann, *Structure and Dynamics of Membranes, Handbook of Biological Physics: Volume 1* (Elsevier, Amsterdam 1995).
2. P. Walde, M. Wessicken, U. Raedler, N. Berclaz, K. Conde-Frieboes, and P. L. Luisi, J. Phys. Chem. **101**, 7390 (1997).
3. B. zu Putlitz, K. Landfester, S. Foerster, and M. Antonietti, Langmuir **16**, 3003 (2000).
4. B. M. Discher, D. A. Hammer, F. S. Bates, and D. E. Discher, Current Opinion in Colloid and Interface Science **5**, 125 (2000).
5. R. Lipowsky, *From Membranes to Membrane Machines, Statistical Mechanics of Biocomplexity* (Springer, Berlin 1999).
6. H-G. Doebereiner, O. Selchow, and R. Lipowsky, Eur. Biophys. J. **28**, 174 (1999).
7. D. Needham and R. S. Nunn, Biophys. J. **58**, 997 (1990).
8. A. Sonnleitner, G. J. Schuetz, and Th. Schmidt, Biophys. J. **77**, 2638 (1999).
9. R. Dimova, C. Dietrich, A. Hadjiisky, K. Danov, and B. Pouligny, Eur. Phys. J. B **12**, 589 (1999).
10. W. Rawicz, K. C. Olbrich, T. McIntosh, D. Needham, and E. Evans, Biophys. J. **79**, 328 (2000).
11. D. Harries, and A. Ben-Shaul, J. Chem. Phys. **106**, 1609 (1997).
12. R. Goetz and R. Lipowsky, J. Chem. Phys. **108**, 7397 (1998).
13. R. Goetz, G. Gompper and R. Lipowsky, Phys. Rev. Lett. **82**, 221 (1999).
14. E. Lindahl and O. Edholm, Biophys. J. **79**, 426 (2000).
15. J. C. Shelley, M. Y. Shelley, R. C. Reeder, S. Bandyopadhyay, and M. L. Klein, J. Phys. Chem. B **105**, 4464 (2001).
16. P. J. Hoogerbrugge and J. M. V. A. Koelman, Europhys. Lett. **19**, 155 (1992).
17. R. D. Groot and P. B. Warren, J. Chem. Phys. **107**, 4423 (1997).
18. P. B. Warren, Current Opinion in Colloid and Interface Science **3**, 620 (1998).
19. R. S. Cantor, Biophys. J. **76**, 2625 (1999).
20. P. Schofield and J. R. Henderson, Proc. R. Soc. Lond. **A379**, 231 (1982).